

**Ion separation effects in mixed-species ablators for inertial-confinement-fusion implosions**Peter Amendt,<sup>\*</sup> Claudio Bellei,<sup>†</sup> J. Steven Ross, and Jay Salmonson  
*Lawrence Livermore National Laboratory, Livermore, California 94551, USA*

(Received 15 October 2014; published 6 February 2015)

Recent efforts to demonstrate significant self-heating of the fuel and eventual ignition at the National Ignition Facility make use of plastic (CH) ablators [O. A. Hurricane *et al.*, *Phys. Plasmas* **21**, 056314 (2014)]. Mainline simulation techniques for modeling CH capsule implosions treat the ablator as an average-atom fluid and neglect potential species separation phenomena. The mass-ablation process for a mixture is shown to lead to the potential for species separation, parasitic energy loss according to thermodynamic arguments, and reduced rocket efficiency. A generalized plasma barometric formula for a multispecies concentration gradient that includes collisionality and steady flows in spherical geometry is presented. A model based on plasma expansion into a vacuum is used to interpret reported experimental evidence for ablator species separation in an inertial-confinement-fusion target [J. S. Ross *et al.*, *Rev. Sci. Instrum.* **83**, 10E323 (2012)]. The possibility of “runaway” hydrogen ions in the thermoelectric field of the ablation front is conjectured.

DOI: [10.1103/PhysRevE.91.023103](https://doi.org/10.1103/PhysRevE.91.023103)

PACS number(s): 52.27.Cm, 47.32.Ef, 52.38.Ph, 52.57.–z

**I. INTRODUCTION**

Efforts to demonstrate significant fuel self-heating [1], thermonuclear breakeven and ignition on the National Ignition Facility (NIF) continue in earnest [2]. A plastic (CH) capsule ablator absorbs soft x rays generated in a high-Z cylindrical enclosure (or hohlraum) that is heated by up to 1.9 MJ of 0.351- $\mu\text{m}$  laser light. In direct reaction to the x-ray-driven ablation, the remainder of the shell inwardly accelerates and compresses an encapsulated deuterium (D) and tritium (T) fuel mixture to thermonuclear conditions.

Experiments on the NIF dedicated to measuring the peak implosion speed of the imploding CH shell with x-ray backlighting techniques have consistently shown a  $10\% \pm 5\%$  deficit compared with radiation-hydrodynamic (RH) simulation predictions [3]. Explanations for this discrepancy range from equation-of-state uncertainties for CH, higher-than-expected x-ray albedo of the CH ablator, reduced hohlraum coupling to the capsule from anomalous laser backscatter phenomena, to reduced laser (gas-filled) hohlraum coupling near peak power. If an anomalously low coupling efficiency is responsible for the observed shortfall in peak implosion speed to within  $5\% \pm 5\%$  of what is required for ignition ( $\sim 370 \mu\text{m/ns}$ ), the expectation is that this deficit can be overcome with higher laser powers ( $\sim 500 \text{ TW}$ ) and the use of depleted uranium hohlraums [4]. Indeed, a recent high power (520 TW) and energy (1.86 MJ) shot with a uranium hohlraum appears to have demonstrated the required peak implosion velocity and remaining ablator mass above the ignition goal [5]. Dedicated “ViewFactor” hohlraum experiments have since established that much of this inferred drive deficit is due to an (as yet) unidentified mechanism for reduced laser-hohlraum coupling [6] and can “explain nearly all of the disagreement with the velocity data.” However, multi-ion species capsules may still be subject to a modest degree of separation phenomena that degrade performance through an

energy expense from transiently lower entropy, motivating the use of potentially more efficient ablator materials such as high-density carbon (HDC)—which is also being explored on the NIF [7].

An often-overlooked physical phenomenon in inertial-confinement fusion (ICF) is the potential for species separation from acceleration-induced pressure gradients, self-generated electric fields, and temperature gradients. In the case of CH ablators, the large ion mass ratio of carbon to hydrogen ( $\sim 12$ ) allows the possibility of barodiffusion-driven species separation [8–12]. Similarly, the significant difference in charge-to-mass ratios for (fully ionized) C and H may allow electrodiffusion-mediated species separation to occur as well [9–12]. Recent work has shown that electron and ion thermodiffusion may be particularly important for ICF plasmas, potentially dominating over barodiffusion and electrodiffusion [13]. Under warm-dense matter conditions near an ablation front, diffusive time scales are often long relative to an implosion time scale, but strong pressure and temperature gradients and electric fields ( $> 10^4 \text{ statvolts/cm}$ ) may still drive an appreciable separation of species occurring well within an implosion time [9]. This physical feature is analogous to the species segregation that takes place in the upper atmosphere above the turbopause where the standard barometric formula corrected for buoyancy applies [14].

In this article thermodynamic arguments are developed to show that an ablating mixed-species shell may lead to an energy loss in the process of separating the constituent ions. The rocket efficiency of a mixed-species ablator is calculated to decrease due to the difference in exhaust speeds of the constituent ions (leading to species separation). Direct evidence for significant species separation is known based on Thomson scattering measurements of a direct-drive  $\text{CH}_2$  planar sample [15]. A simple model based on plasma expansion into a vacuum is applied to interpret the observed species separation. The possibility of “runaway” hydrogen ions from a thermoelectric field at the head of the ablation front is also conjectured and shown to be consistent with the observed species separation. The main conclusion of this work is that mainline (single) fluid-based simulation techniques used in ICF studies currently neglect potential species separation

<sup>\*</sup> amendt1@llnl.gov<sup>†</sup>Present address: Centre Laser Intenses et Applications, Université de Bordeaux, UMR 5107, F-33405 Talence, France.

phenomena, thereby motivating adaptations of these standard RH tools, use of multifluid particle-in-cell (PIC) simulation techniques [16], or the simplifying option of single-species ablators such as HDC and aluminum.

## II. MULTISPECIES ABLATOR ROCKET EFFICIENCY

Some physical insight into why average-atom RH simulations may overestimate (areal) mass-ablation rates in a mixed-species ablator can be gained as follows. Consider a dissociated pair of C and H atoms, each born with an average thermal energy of  $3k_B T/2$  and ideally converted into radially directed kinetic energy  $m_j v_j^2/2$  at a hypothetical ablation front, where  $k_B$  is Boltzmann's constant,  $T$  is the temperature, and the species label  $j = C$  or  $H$ . If each atom is allowed to move at its own separate velocity, the momentum for this pair of atoms follows as  $p_{\text{sep}} = m_H v_H + m_C v_C = \sqrt{3k_B T}(\sqrt{m_H} + \sqrt{m_C})$ . On the other hand, RH simulations force the H and C atoms to move together in an average-atom sense such that  $3k_B T = (m_H + m_C)\bar{v}^2/2$ , where  $\bar{v}$  is the average fluid speed. The resulting momentum for this average atom follows as  $p_{\text{RH}} = (m_H + m_C)\bar{v} = \sqrt{6k_B T(m_H + m_C)}$ . Forming the ratio of the two momenta gives  $p_{\text{RH}}/p_{\text{sep}} = \sqrt{2(m_H + m_C)}/(\sqrt{m_H} + \sqrt{m_C})$ , which equals 1.1422. By not allowing the H and C atoms to physically separate, the RH simulation tools may be overestimating the mass-ablation rate by nearly 14% according to this argument.

The CH ablator used in ignition and alpha heating studies on the NIF to date have contained buried mid-Z dopant layers as well, e.g., 1.0 at. % Ge or 2.0 at. % Si, to control x-ray preheat of the interior DT fuel [17]. Adapting the above argument to the case of 1.0 at. % Ge in CH shows that RH codes may overestimate the momentum transferred to the shell from ablating  $\text{CH}_{0.98}\text{Ge}_{0.02}$  by over 16%.

An ablating ICF shell is necessarily in a plasma state, and revisions of the above argument are necessary. Accordingly, we start with a rocket model for the ablating shell:  $M\dot{v} = -v_E \dot{M}$ , where  $M$  is the remaining shell mass,  $\dot{v}$  is the shell acceleration,  $v_E = 2\sqrt{(Z+1)k_B T/Am_H}$  is the exhaust speed [18],  $Z$  is the ionization state of the ablated ion and  $A$  its atomic mass number. For a composite ablator material or mixture, e.g., CH, we form the mass-weighted exhaust speed  $\bar{v}_E \equiv \alpha v_{E,1} + (1-\alpha)v_{E,2}$ , where  $\alpha$  is the ratio of light-ion mass density to the total mass density. The rocket efficiency  $\eta$  is defined as the ratio of shell kinetic energy to the exhaust energy:

$$\eta \equiv \frac{E_{\text{kin}}}{E_{\text{ex}}} = \frac{M[\ln(M/M_0)]^2}{(M_0 - M)} \left\{ \frac{[\alpha v_{E,1} + (1-\alpha)v_{E,2}]^2}{\alpha v_{E,1}^2 + (1-\alpha)v_{E,2}^2} \right\}, \quad (1)$$

where  $M_0$  is the initial shell mass. The expression in braces in Eq. (1) describes the change in rocket efficiency from differences in the exhaust speeds of the constituent ions. The difference in exhaust speeds at the ablation front can lead to a transient species separation, but interspecies collisions may alone suppress the separation downstream of the ablation front (See Sec. III) and nullify any potential decrease in rocket efficiency. Thus, Eq. (1) represents an upper bound on rocket efficiency degradation if the ions remain asymptotically separated away from the capsule payload. Figure 1 depicts the rocket efficiency decrease in a CH ablator as a function of

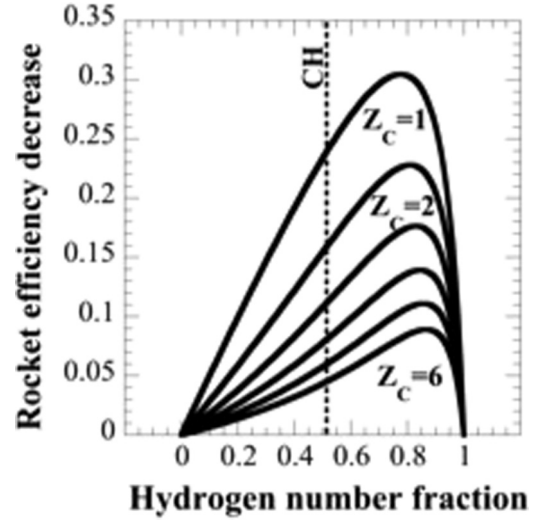


FIG. 1. Fractional decrease in rocket efficiency versus hydrogen number fraction in CH ablator for various ionization states of carbon based on Eq. (1). Vertical dashed line denotes initial composition of CH ablator.

hydrogen number fraction and the possible ionization states of carbon. Even for equimolar concentrations of hydrogen and carbon, i.e., no residual species separation, a several-percentage effect is predicted. In indirect-drive implosions the ionization state of carbon near the head of the ablation front is in the range of 4–5, giving a nearly 6%–8% decrease in rocket efficiency for CH compared with an “average-atom” ablator. A further decrease in rocket efficiency is predicted for doped ablators as well. Generalizing Eq. (1) to three species for a 1.0 at. % Ge doping of CH shows that the rocket efficiency is further degraded, giving a value of 9.4% (8.2%) for  $Z_{\text{Ge}} = 9$  and  $Z_C = 4$  (5). Clearly, the difference in exhaust speeds (at asymptotic distances from the ablation front) between the two ion species is what drives the reduced rocket efficiency according to Eq. (1). In Sec. IV we assess the experimental evidence and develop theoretical arguments for such an asymptotic difference in exhaust speed (or associated species separation). Use of the rocket model is meant only as a guide to assessing changes in the rocket efficiency arising from an asymptotic species separation. Ultimately, inclusion of the detailed microphysics of the ablation process with PIC or molecular dynamics simulations is needed before rendering any firm conclusions on the quantitative role of species separation on rocket efficiency.

RH simulations with many alternating ( $\sim$ micron thick) layers of pure C and H can be used to assess the impact of an imposed species separation on the average hydrodynamics of an indirect-drive implosion (but without interspecies penetration). By imposing the constraints of equal areal mass density:  $\rho_H \Delta_H + \rho_C \Delta_C = \rho_{\text{CH}}(\Delta_H + \Delta_C)$ , and equal areal atomic number density in the RH simulation:  $n_H \Delta_H = n_C \Delta_C$ , the prescribed relative layer thicknesses and mass densities (in the direction of ablative expansion) are derived:

$$\frac{\Delta_C}{\Delta_H} = \frac{A_C \rho_{\text{CH}} / \rho_C}{1 + A_C (1 - \rho_{\text{CH}} / \rho_C)}, \quad (2a)$$

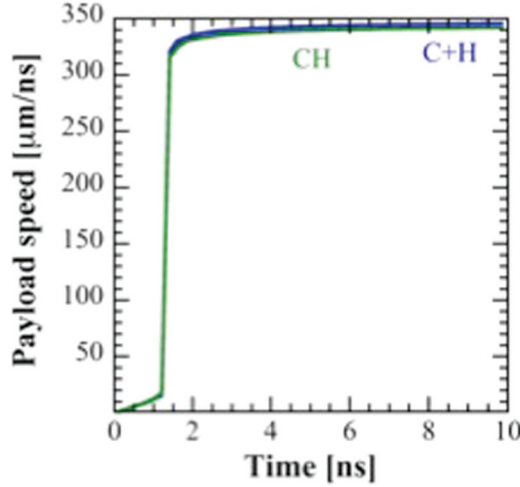


FIG. 2. (Color) Simulated 5- $\mu\text{m}$ -thick CH payload velocity versus time driven by a 1-ns 200-eV radiation temperature source acting on fully mixed CH ablator (green) and segregated H+C layers (blue) where thickness of H layers is 1  $\mu\text{m}$  and total thickness of ablator is 91.2  $\mu\text{m}$ .

$$\frac{\rho_H}{\rho_{CH}} = 1 + \frac{\Delta_C}{\Delta_H} \left( 1 - \frac{\rho_C}{\rho_{CH}} \right), \quad (2b)$$

where  $\Delta_H(\Delta_C)$  is the thickness of the hydrogen (carbon) layer,  $\rho_H(\rho_C)$  is the mass density of the hydrogen (carbon) layer,  $n_H(n_C)$  is the number density of the hydrogen (carbon) layer, and  $A_C$  is the atomic weight of carbon. The mass density of CH is chosen as 1.05 g/cm<sup>3</sup>, and the density of the graphite (an allotrope of carbon)  $\rho = 2.2$  g/cm<sup>3</sup>. Figure 2 shows that the average one-dimensional hydrodynamics as described by the trajectory of an x-ray-driven planar sample is hardly affected by separation. However, energy must be expended to realize such a configuration of lower entropy based on thermodynamic principles, which we now estimate.

### III. THERMODYNAMICS OF SPECIES SEPARATION

The energy expended in segregating an initially homogeneous plasma mixture follows from thermodynamic arguments. It is well known that energy must be invested to change the concentration of a solution by reducing or removing the solvent [14], and the same principle carries over to driven species separation across an ablation front. To this end, the thermodynamic potential  $\Xi$  (or Legendre transform of the energy with respect to entropy and volume) is a suitable starting point. Figure 3 schematically shows two configurations of a CH plasma mixture, for which we calculate the change in thermodynamic potential (or Gibbs free energy)  $\Delta\Xi$  from an initially mixed state (left) to a partially segregated one (right), assuming constant temperature and pressure conditions and ideal gas behavior [14]:

$$\Delta\Xi[kJ] = 16.0 \left[ \frac{N_i}{10^{20}} \right] T_i[\text{keV}] \times [\ln 2 + c \ln c + (1-c) \ln(1-c)], \quad (3)$$

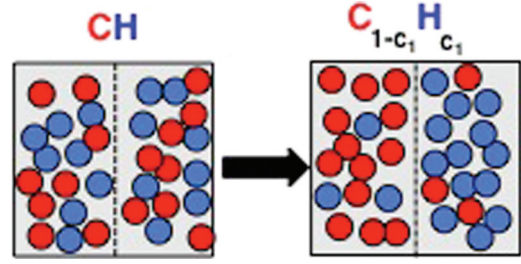


FIG. 3. (Color) Schematic of fully mixed C and H sample (left) and partially mixed sample (right) for calculating change in thermodynamic potential [Eq. (3)].

where  $N_i$  is the number of ablator ions, and  $c$  is the number fraction of H ions. Equation (3) assumes that the constituent ion species have the same temperature, although recent work based on multifluid simulations has established that *shock-driven* species separation can lead to different ion temperatures [19]. To what extent the dynamics of ablation can lead to dissimilar ion temperatures and potentially affect species separation must await PIC simulation studies.

Figure 4 shows the separation energy as a function of hydrogen concentration at 1 keV,  $N_i = 1.5 \times 10^{20}$  for the case of direct drive (or, equivalently, 0.3 keV,  $N_i = 5 \times 10^{20}$  for indirect drive), indicating a significant amount of energy when the ion separation is significant. NIF implosion experiments consistently show a nearly 15%–25% deficit in (inferred) absorbed capsule energy compared with the nominal level of  $\sim 170$  kJ [20]. However, dedicated “ViewFactor” hohlraum experiments have established that much of this deficit is due to an (as yet) unidentified mechanism for reduced laser-hohlraum coupling [6], allowing still for a possible role of separation energy losses in the implosion dynamics. By comparison, direct-drive implosions are less susceptible to this separation energy loss, owing to the relatively fewer number of ablator ions (due to the low ablation front speed) and the high laser

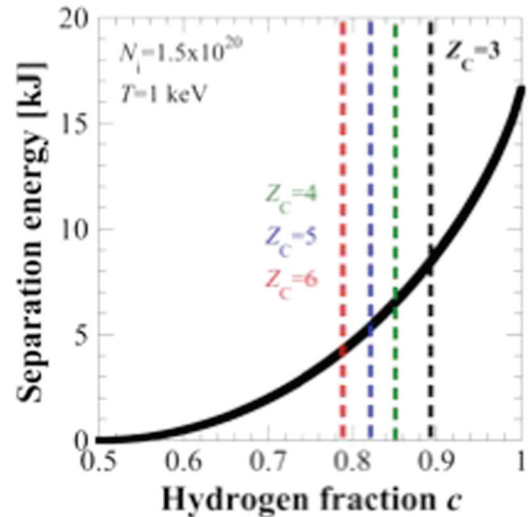


FIG. 4. (Color) Separation energy versus hydrogen concentration and indicated candidate carbon ionization states: 6 (red), 5 (blue), 4 (green), and 3 (black), according to Eq. (3).

coupling efficiency to the capsule ( $\sim 60\%$ ); i.e., fractionally lower separation losses are expected.

#### IV. STEADY-STATE ABLATOR SPECIES SEPARATION

To estimate the degree of species separation, we compare the thickness of a steady-state ablation front with the constituent ion mean-free-path lengths and the hydrodynamic scale length  $\sim C_s t$ , where  $C_s$  is the isothermal sound speed. For direct drive, the ablation front thickness is an appropriately defined fraction of the conduction layer [18], determined by the requirement that the ablation front thickness should be on the order of an average-ion mean free path [21,22]. That is, if the ablation front is modeled as a discontinuity in the plasma flow properties, a mean-free-path assertion on the width becomes tenable—in analogy with the Rankine-Hugoniot jump conditions applied to a fluid shock. The conduction layer temperature profile is a strongly nonlinear function of position near the head of the layer ( $x \cong x_c$ ), varying as  $T(x) = T_c(1 - x/x_c)^{2/5}$ , where  $T_c$  is the channel temperature (typically  $>1$  keV for  $0.35\text{-}\mu\text{m}$  wavelength incident frequency-converted laser light or “ $3\omega$ ”) and

$$x_c[\mu\text{m}] = 17.4\bar{A}^{1/2}T_c^2[\text{keV}] \frac{(\bar{Z} + 0.24)}{(1 + \bar{Z})^{3/2}(1 + 0.24\bar{Z})\ln\Lambda_{ei}}, \quad (4)$$

where  $\bar{A}$  is the average-ion atomic number,  $\bar{Z}$  is the average-ion charge state, and  $\ln\Lambda_{ei}$  is the electron-ion Coulomb logarithm. Note that the nonlinear heat wave solution  $T(x)$  has an unbounded temperature gradient at  $x = x_c$ . The *width* of the ablation front  $\Delta_a$  is defined as the distance from the head of the ablation front ( $x = x_c$ ) to a downstream position ( $x = x_c - \Delta_a$ ) such that  $\Delta_a$  is an *average-ion* mean free path. This condition gives a temperature at the rear ( $x = x_c - \Delta_a$ ) of the ablation front layer of nearly  $T_c/10$ , corresponding to a  $\bar{Z} \sim 2.5$ , after choosing  $n_i \sim 10^{23}\text{ cm}^{-3}$  for solid density CH. A criterion for significant species separation over an ablation front is when the mean-free-path length for a hydrogen-carbon

collision  $\lambda_{\text{HC}} \propto Z_C^{-2}$  exceeds the ablation front width. More precisely, we define the degree of ablation front species separation as  $c = 1 - \max(\Delta_a, \lambda_{\text{CC}})/2\max(\Delta_a, \lambda_{\text{HC}})$ , where  $\lambda_{\text{CC}} \propto Z_C^{-4}$  is the carbon-carbon mean free path. In this way minimal species separation occurs if  $\Delta_a \cong \lambda_{\text{HC}}$ , and maximum separation is found when  $\Delta_a \cong \lambda_{\text{CC}}$ . Figure 4 shows estimates of the expected degree of incipient species separation for various carbon charge states  $Z_C$  based on ratios of mean free paths to an ablation front thickness scale. However, because  $\Delta_a \ll x_c$ , scattering processes are expected to degrade any species separation (localized to the ablation front) over a conduction scale length and beyond, e.g., a hydrodynamic or observation scale length (see below). Nonetheless, the transient separation that takes place on the order of an ablation front width may lead to an expenditure of (separation) energy according to Eq. (3) on the order of several kilojoules.

From a strict hydrodynamic standpoint, species separation across the ablated plasma can be shown to rapidly dissipate due to collisions, despite the segregating influence of strong pressure gradients and self-generated electric fields. Accordingly, we consider the steady-state momentum balance for H and C ions, coupled with mass conservation:

$$v_{\text{H}}v'_{\text{H}} = -P'_{\text{H}}/\alpha\rho + Z_{\text{H}}eE/m_{\text{H}} - v_{\text{HC}}(v_{\text{H}} - v)/(1 - \alpha), \quad (5a)$$

$$vv' = P'/\rho, \quad (5b)$$

$$v'_{\text{H}} - v' = -(v_{\text{H}} - v)[\rho'/\rho + 2/r] - v_{\text{H}}\alpha'/\alpha, \quad (5c)$$

where primes denote the spatial derivative,  $P_{\text{H}}$  is the hydrogen pressure,  $\rho$  is the total mass density,  $v_{\text{HC}}$  is the hydrogen-carbon collision frequency,  $P$  is the total pressure,  $v \equiv \alpha v_{\text{H}} + (1 - \alpha)v_{\text{C}}$  is the mass-weighted fluid speed,  $r$  is the spherical radial coordinate, and quasi-neutrality is assumed to hold to a good approximation. In the limit of high collisionality ( $v_{\text{HC}} \rightarrow \infty$ ),  $v_{\text{H}} \rightarrow v$  and the separation vanishes ( $\alpha' \rightarrow 0$ ) when  $v'_{\text{H}} - v' \rightarrow 0$  also. Combining Eqs. 5(a) and 5(b) and using  $E = (k_{\text{B}}T/e)\{-P'/P + \alpha'\Delta Z/D[(1 - \alpha)Z_{\text{C}} + \alpha Z_{\text{H}}m_{\text{C}}/m_{\text{H}}]\}$  [8], we find

$$\alpha' = \frac{\alpha(v' - v'_{\text{H}})v_{\text{HC}} + \alpha(1 - \alpha)(\nabla\ln\rho + 2/r)[P'(1 + Z_{\text{H}} - D)/\rho D - (vv' - v_{\text{H}}v'_{\text{H}})]}{v_{\text{H}}v_{\text{HC}} - (1 - \alpha)(\nabla\ln\rho + 2/r)\left(\frac{P}{\rho D^2}\right)\left(\frac{m_{\text{H}}}{m_{\text{C}}}\right)\left\{D + \alpha\Delta Z - \frac{\alpha\Delta Z}{[\alpha Z_{\text{H}} + (1 - \alpha)Z_{\text{C}}m_{\text{H}}/m_{\text{C}}]}\right\}}, \quad (6)$$

where  $D \equiv \alpha(1 + Z_{\text{H}}) + (1 - \alpha)(1 + Z_{\text{C}})m_{\text{H}}/m_{\text{C}}$ , and the usual plasma barometric formula [ $\alpha' = k_{\alpha}(\alpha; Z_{\text{H}}, Z_{\text{C}}, m_{\text{H}}, m_{\text{C}})P'/P$ ] is recovered in the limit of  $v = v_{\text{H}} = 0$ ,  $v' = v'_{\text{H}}$  [8]. Equation (6) represents a generalization of the plasma barometric formula [9] to include steady-state spherical flows with arbitrary collisionality. Application of Eq. (6) to ICF implosions where the average-ion fluid profiles  $\{v_{\text{HC}}, P, v, \rho\}$  are obtained from RH simulations of imploding capsules can be shown to lead to negligible species stratification across the ablated plasma over a large range of times. This result is consistent with a previous fluid-based analysis of laser-produced plasmas [23]. Thus, the possibility of laser-produced species separation persisting beyond an ablation front requires a nonfluid, plasma-based scenario.

For a laser-produced plasma expanding into a near vacuum as in direct drive, the highly mobile electrons advance into the vacuum region over a Debye length scale to create an ambipolar, accelerating electric field for the ablating ions. Moreover, the thermoelectric field [ $E_{\text{T}} = 0.71(k_{\text{B}}/e)\nabla\ln T_e$ ] produced at the head of the ablation front ( $x = x_c$ ) typically exceeds the threshold value for an electron runaway electric field, defined as the threshold value for accelerating an electron by a thermal speed over an electron-electron collision time [24]:  $E_r^{(e)} = 0.266e\ln\Lambda/\lambda_{\text{De}}^2$ , where  $\Lambda = 12\pi n\lambda_{\text{De}}^3/Z$  [25]. For the conditions near the head of the ablation region described earlier ( $T_e \sim 100\text{ eV}$ ,  $n_e \sim 10^{23}\text{ cm}^{-3}$ ), the electron runaway electric field  $\cong 7 \times 10^9\text{ V/m}$  is appreciably less than a thermoelectric field strength  $E_{\text{T}}$  of  $\cong 3 \times 10^{10}\text{ V/m}$ . For hydrogen ions, the runaway field condition is primarily

determined by the hydrogen-carbon collision rate, giving

$$E_r^{(H)} = \frac{Z_C^2}{1 + Z_C} \left( \frac{m_C}{m_H + m_C} \right)^{1/2} 0.266e \ln \Lambda_{HC} / \lambda_{De}^2. \quad (7)$$

For  $Z_C \sim 4$  the runaway electric field for hydrogen ions is still less than the thermoelectric field strength, allowing for the possibility of escaping ions. On the other hand, the carbon ions are not able to run away due to the stronger scaling with  $Z_C$  of the carbon runaway field  $E_r^{(C)} = 0.266e \ln \Lambda_C Z_C^2 / (1 + Z_C) \lambda_{De}^2$ . Thus, a physical mechanism for species separation occurring at the ablation front and persisting throughout the downstream flow is plausible, according to this nonfluid (plasma) scenario.

Another physical picture for incorporating self-induced electric fields in the dynamics of a laser-ablated plasma is the freely expanding plasma model. According to this approach, the location of the ion front is conventionally defined where the local Debye length coincides with the hydrodynamic scale length [26–28], giving for the asymptotic ion front velocity versus time,

$$v_\alpha \cong C_{s\alpha} (2 \ln \omega_{p\alpha} t + 1), \quad (8)$$

where  $\omega_{p\alpha} = \sqrt{4\pi n_e Z_\alpha e^2 / m_\alpha}$  is the ion plasma frequency for species  $\alpha$  and  $C_{s\alpha} = \sqrt{Z_\alpha k_B T_e / m_\alpha}$  is the ion-acoustic speed. Equation (8) should be compared with the *self-similar* hydrodynamic solution for the ion front speed:  $v_a \cong C_{s\alpha} \ln \omega_{p\alpha} t$ . The difference arises from a twofold enhancement of the electric field localized to the ion front over a length scale on the order of  $C_{s\alpha} t$  [27].

There is recent experimental evidence for significant species separation in CH<sub>2</sub> planar foils fielded on the Omega Laser Facility [29], according to Thomson scattering measurements of collective electron-plasma and ion-acoustic fluctuations [14]. The CH<sub>2</sub> foil is directly heated with 10 laser beams with 5 kJ total energy at  $3\omega$  (0.35- $\mu$ m wavelength), and Thomson scattering is measured 4 mm from the foil surface using a 30-J,  $2\omega$  probe laser with a 1-ns pulse length. Using a series of target shots the plasma evolution is measured from 2.5 to 9 ns after the rise of the heater beams. Measuring the electron density and temperature from the electron-plasma fluctuations constrains the fit of the two ion species theoretical form factor [30] for the ion feature such that the ion temperature, plasma flow velocity, and ion species fraction are determined. The ion species fraction is determined to an accuracy of  $\pm 6\%$ . Figure 5 shows the inferred species fraction history with a significant hydrogen fraction persisting beyond 6 ns before the ablated carbon starts to appreciably enter the Thomson scattering volume. This is direct evidence of species separation in an ICF-relevant experiment.

A model for interpreting the delay in carbon ions arriving in the Thomson scattering volume in terms of runaway hydrogen ions can be obtained as follows. First, the average flow velocity (or exhaust speed) was measured to decrease linearly with time:  $\bar{v}_E(t) = v_0 t_0 / t$ , where  $t_0$  is the laser pulse duration ( $\sim 1$  ns) and  $v_0$  is the average-ion exhaust speed at  $t_0$ . This behavior is corroborated by a self-similar analysis for  $v \equiv r/t$ , giving  $\vec{\nabla} \cdot \vec{v} \equiv 3/t$  [29]. From an analysis of stationary laser-driven ablation [18], the peak channel temperature  $T_c$  [keV] =  $13.7(I/[10^{15} \text{ W/cm}^2] \lambda_{3\omega}^2 / [\mu\text{m}])^{2/3}$  is found. The overlapped

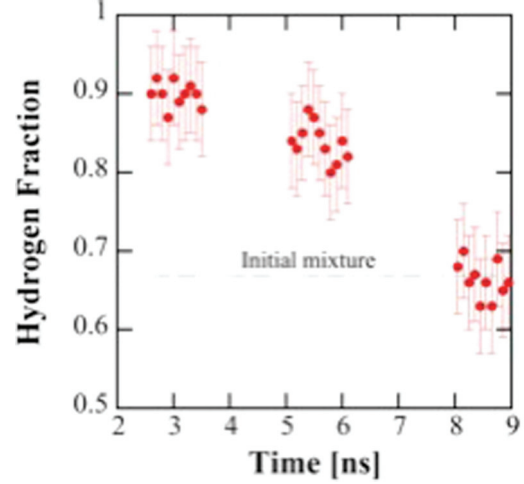


FIG. 5. (Color) Inferred hydrogen number fraction from Thomson scattering measurements 4 mm in front of CH<sub>2</sub> sample versus time relative to start of laser pulse (1 ns flat-top).

beam intensity in the experiment is nearly  $10^{16} \text{ W/cm}^2$  [31], giving a peak ablation channel temperature of nearly 16 keV at  $t = t_0$ . From this behavior the hydrogen exhaust speed follows:  $v_E^{(H)} = (1 + 2\sqrt{2}) \sqrt{k_B T / m_H t_0} / t$ , where the increase in hydrogen ion speed by one unit of thermal speed due to runaway fields at the ablation front is explicitly included. The arrival time of the hydrogen is given by  $t_a^{(H)} = x_{\text{exp}} / \bar{v}_E^{(H)}$ , where  $\bar{v}_E^{(H)} = (t_a^{(H)} - t_0)^{-1} \int_{t_0}^{t_a^{(H)}} dt v_E^{(H)}(t)$  is the time-averaged hydrogen exhaust speed and  $x_{\text{exp}} = 4$  mm is the distance of the Thomson scattering volume from the initial CH<sub>2</sub> position. Solving for  $t_a^{(H)}$  gives an arrival time of just under 1 ns, or well before the first observation time of  $\sim 2.5$  ns. Similarly, the arrival time of the carbon ions  $t_a^{(C)} = x_{\text{exp}} / \bar{v}_E$  is associated with the average exhaust speed  $\bar{v}_E(t) = 2\sqrt{(\bar{Z} + 1)k_B T / \bar{A} m_H t_0} / t$ , where  $\bar{Z} = 8/3$  and  $\bar{A} = 14/3$  for CH<sub>2</sub> are taken. Solving iteratively for  $t_a^{(C)}$  gives an arrival time for the first carbon ions  $\sim 6$  ns—close to what was observed.

Equation (8) can be used to independently estimate the arrival time of the hydrogen ion front in the Thomson scattering volume. The electron temperature of  $\sim 100$  eV near the ablation front gives a hydrogen ion-acoustic speed of  $\sim 10^7$  cm/s, leading to an arrival time of  $\sim 1.5$  ns from Eq. (8). The carbon ions lag the hydrogen ions due to their smaller charge-to-mass ratio and are not subject to the Debye length condition that underlies Eq. (8). In other words, the carbon ions are not expanding into a vacuum but instead are preceded by the hydrogen-rich expanding plasma. Thus, the self-similar version of Eq. (8) more appropriately applies to the ablating carbon ion front with its characteristic  $2\times$  smaller electric field. Taking  $Z_C \cong 4$  for carbon at  $\sim 100$  eV, the arrival time for carbon ions is predicted to be near 6 ns, which is consistent with the data.

For indirect drive, the energy deposited behind the ablation front directly arises from bound-free absorption of  $\sim 1$ -keV x rays in a  $\sim 300$ -eV hohlraum [16]. As before, i.e., direct drive, we stipulate that the ablation front thickness is on the order of an average-ion mean free path and is situated at the

leading edge of the absorption region. The absorption region is distributed over a distance on the order of  $1/\kappa\rho$ , where  $\kappa = O(10^3)$  cm<sup>2</sup>/g is the bound-free opacity [18]. The scale length of this absorption region is typically on the order of 10 microns, analogous to the conduction zone of direct drive. Collisions will suppress any incipient species separation at the ablation front as before, and (nonhydro) plasma-induced electric fields on the “plasma vacuum” boundary or runaway fields are required to provide a source of species separation as in direct drive. In contrast to direct drive, there is no confirming experimental evidence for ablator species separation in indirect drive to date.

A further consequence of potential species separation in the ablator is the possibility for differential x-ray absorption in a converging geometry. Consider two contiguous spherical shells of thickness  $\Delta$  and inner radius  $r_0$  of the interior (carbon-rich) shell. Using that the areal mass-ablation rate  $\dot{m}$  scales as the incident x-ray flux to the  $\frac{3}{4}$  power [32] and neglecting the opacity of the hydrogen in the shells, we obtain for the differential change in areal mass-ablation rate from the combined effects of spherical geometry and species separation

$$\frac{\delta\dot{m}}{\dot{m}} = -\frac{3}{4}\left(\frac{\Delta}{r_0}\right)^2\left(1 + \frac{\Delta}{r_0}\right)(2c - 1), \quad (9)$$

where  $c$  is the hydrogen fraction in the outer shell. Thus, a reduced x-ray flux at the ablation front ( $r = r_0$ ) arises from a surplus of carbon in the adjacent spherical layer. For a shell aspect ratio  $r_0/\Delta = 3$  and  $c = 0.8$ , the fractional loss in areal mass-ablation rate is  $\cong 6.7\%$ . A reduced ablation rate translates into a deficit of peak implosion speed  $v_{\text{imp}}$  of nearly 2%, using the scaling relation for indirect drive:  $v_{\text{imp}} \approx \dot{m}^{0.3}$  [32].

## V. SUMMARY

In summary, thermodynamic arguments are used to show that an ablating mixed-species shell leads to an energy loss in the process of separating the constituent ions. The presence of

multispecies ions may lead to differences in the exhaust velocity and a calculated reduction in rocket ablation efficiency, provided species separation persists well beyond the ablation zone. Direct evidence for significant species separation well beyond the ablation zone is provided based on Thomson scattering measurements of a direct-drive CH<sub>2</sub> planar sample. A model based on plasma expansion into a vacuum is used to capture the main features of the data. A scenario for species separation based on thermoelectric fields at the ablation front exceeding the runaway electric field threshold for hydrogen ions (but not carbon ions) is also described. A further effect of species separation is the possibility for a reduced mass-ablation rate in a converging geometry. The main message of this article is that mainline (single) fluid-based simulation techniques currently neglect species separation phenomena, thereby requiring adaptations of these standard RH tools, use of multifluid or hybrid PIC simulation techniques, or the simplifying option of single-species ablaters, e.g., HDC or Al. Work is planned to adapt the multispecies PIC simulation code LSP for assessing multispecies effects on rocket ablation efficiency in x-ray drive. However, the ablation front generally occurs in the warm-dense matter regime, where particle correlations become paramount and the standard plasma transport coefficients and collision operators do not strictly hold. Thus, PIC-based methods as well as Fokker-Planck treatments assume an obvious risk when being applied in such a regime of arguable validity. The microphysics of the ablation process is likely more amenable to molecular dynamics methods, but with an attendant constraint on accessible spatial and temporal scales.

## ACKNOWLEDGMENTS

Useful discussions with Siegfried Glenzer and Scott Wilks are gratefully acknowledged. This work was performed under the auspices of Lawrence Livermore National Security, LLC (LLNS) under Contract No. DE-AC52-07NA27344 and supported by LDRD-11-ERD-075.

- 
- [1] O. A. Hurricane, D. A. Callahan, D. T. Casey, P. M. Celliers, C. Cerjan, E. L. Dewald, T. R. Dittrich, T. Doppner, D. E. Hinkel, L. F. Berzak Hopkins *et al.*, *Nature* **506**, 343 (2014); O. A. Hurricane, D. A. Callahan, D. T. Casey, E. L. Dewald, T. R. Dittrich, T. Doppner, M. A. Barrios Garcia, D. E. Hinkel, L. F. Berzak Hopkins, P. Kervin *et al.*, *Phys. Plasmas* **21**, 056314 (2014).
  - [2] J. D. Lindl and E. I. Moses, *Phys. Plasmas* **18**, 050901 (2011).
  - [3] D. G. Hicks, N. B. Meezan, E. L. Dewald, A. J. MacKinnon, R. E. Olson, D. A. Callahan, T. Doppner, L. R. Benedetti, D. K. Bradley, P. M. Celliers *et al.*, *Phys. Plasmas* **19**, 122702 (2012).
  - [4] D. A. Callahan, N. B. Meezan, S. H. Glenzer, A. J. MacKinnon, L. R. Benedetti, D. K. Bradley, J. R. Celeste, P. M. Celliers, S. N. Dixit, T. Doppner *et al.*, *Phys. Plasmas* **19**, 056305 (2012).
  - [5] N. B. Meezan, A. J. MacKinnon, D. G. Hicks, E. L. Dewald, R. Tommasini, S. Le Pape, T. Doppner, T. Ma, D. R. Farley, D. H. Kalantar *et al.*, *Phys. Plasmas* **20**, 056311 (2013).
  - [6] S. A. MacLaren, M. B. Schneider, K. Widmann, J. H. Hammer, B. E. Yoxall, J. D. Moody, P. M. Bell, L. R. Benedetti, D. K. Bradley, M. J. Edwards *et al.*, *Phys. Rev. Lett.* **112**, 105003 (2014).
  - [7] A. J. MacKinnon, N. B. Meezan, J. S. Ross, S. Le Pape, L. Berzak Hopkins, L. Divol, D. Ho, J. Milovich, A. Pak, J. Ralph *et al.*, *Phys. Plasmas* **21**, 056318 (2014).
  - [8] P. Amendt, O. L. Landen, H. F. Robey, C. K. Li, and R. D. Petrasso, *Phys. Rev. Lett.* **105**, 115005 (2010); P. Amendt, S. C. Wilks, C. Bellei, C.K. Li, and R.D. Petrasso, *Phys. Plasmas* **18**, 056308 (2011).
  - [9] P. Amendt, C. Bellei, and S. Wilks, *Phys. Rev. Lett.* **109**, 075002 (2012).
  - [10] G. Kagan and X.-Z. Tang, *Phys. Plasmas* **19**, 082709 (2012).
  - [11] G. Kagan and X.-Z. Tang, *Phys. Rev. Lett.* **109**, 269501 (2012).
  - [12] P. Amendt, C. Bellei, and S. Wilks, *Phys. Rev. Lett.* **109**, 269502 (2012).
  - [13] G. Kagan and X.-Z. Tang, *Phys. Lett. A* **378**, 1531 (2014).

- [14] L. D. Landau and E. M. Lifshitz, *Statistical Physics* (Pergamon, Oxford, 1958), p. 282.
- [15] J. S. Ross, H.-S. Park, P. Amendt, L. Divol, N. L. Kugland, W. Rozmus, and S. H. Glenzer, *Rev. Sci. Instrum.* **83**, 10E323 (2012).
- [16] P. W. Rambo and R. J. Procassini, *Phys. Plasmas* **2**, 3130 (1995); D. R. Welch, D. V. Rose, B. V. Oliver, and R. E. Clark, *Nucl. Instrum. Methods Phys. Res., Sect. A* **464**, 134 (2001); O. Larroche, *Eur. Phys. J. D* **27**, 131 (2003).
- [17] S. W. Haan, J. D. Lindl, D. A. Callahan, D. S. Clark, J. D. Salmonson, B. A. Hammel, L. J. Atherton, R. C. Cook, M. J. Edwards, S. Glenzer *et al.*, *Phys. Plasmas* **18**, 051001 (2011).
- [18] S. Atzeni and J. Meyer-ter-Vehn, *The Physics of Inertial Fusion* (Oxford University Press, Oxford, 2004).
- [19] C. Bellei, H. Rinderknecht, A. Zylstra, M. Rosenberg, H. Sio, C. K. Li, R. Petrasso, S. C. Wilks, and P. A. Amendt, *Phys. Plasmas* **21**, 056310 (2014).
- [20] O. S. Jones, C. J. Cerjan, M. M. Marinak, J. L. Milovich, H. F. Robey, P. T. Springer, L. R. Benedetti, D. L. Bleuel, E. J. Bond, D. K. Bradley *et al.*, *Phys. Plasmas* **19**, 056315 (2012).
- [21] J. J. Duderstadt and G. A. Moses, *Inertial Confinement Fusion* (Wiley & Sons, New York, 1982).
- [22] S. P. Hatchett, Lawrence Livermore National Laboratory Report No. UCRL-JC-108348 (LLNL, Livermore, CA, 1991).
- [23] P. Mulser, *Plasma Phys.* **13**, 1007 (1971).
- [24] J. D. Huba, *NRL Plasma Formulary* (Naval Research Laboratory, Washington, DC, 2011).
- [25] N. Krall and A. Trivelpiece, *Principles of Plasma Physics* (McGraw-Hill, New York, 1973).
- [26] Y. Kishimoto, K. Mima, T. Watanabe, and K. Nishikawa, *Phys. Fluids* **26**, 2308 (1983).
- [27] P. Mora, *Phys. Rev. Lett.* **90**, 185002 (2003).
- [28] S. C. Wilks, A. B. Langdon, T. E. Cowan, M. Roth, M. Singh, S. Hatchett, M. H. Key, D. Pennington, A. MacKinnon, and R. A. Snavely, *Phys. Plasmas* **8**, 542 (2001).
- [29] T. R. Boehly, D. L. Brown, R. S. Craxton, R. L. Keck, J. P. Knauer, J. H. Kelly, T. J. Kessler, S. A. Kumpan, S. J. Loucks, S. A. Letzring *et al.*, *Opt. Commun.* **133**, 495 (1997).
- [30] J. A. Fejer, *Can. J. Phys.* **39**, 716 (1961); D. E. Evans, *Plasma Phys.* **12**, 573 (1970).
- [31] J. S. Ross, S. H. Glenzer, P. Amendt, R. Berger, L. Divol, N. L. Kugland, O. L. Landen, C. Plechaty, B. Remington, D. Ryutov *et al.*, *Phys. Plasmas* **19**, 056501 (2012).
- [32] J. D. Lindl, *Inertial Confinement Fusion* (Springer, New York, 1998), p. 55.